Performance Evaluation of 3D-LOCUS Advanced Acoustic LPS

José Carlos Prieto, Antonio Ramón Jiménez, Jorge Guevara, Joao L. Ealo, Fernando Seco, Javier O. Roa, and Francisco Ramos

***Abstract*—Local Positioning Systems (LPSs) based on acoustic transducers (mainly ultrasonic) offer accurate localization in indoor environments. However, their performance is commonly limited by the transducers' frequency bandwidth and emission pattern. 3D-LOCUS is a new advanced acoustic LPS that claims subcentimeter accuracy even in turbulent environments. This is achieved through the use of broadband omnidirectional transducers, suitable design of emitted signals, proper calibration, and bidirectional emissions. This paper evaluates the 3D-LOCUS LPS by providing results in terms of some positioning metrics such as accuracy, resolution, and coverage, which show how it outperforms other state-of-the-art LPS prototypes. 3D-LOCUS operating in bidirectional mode minimizes environmental effects, such as temperature and airflows, attaining localization errors below 9 mm with a 90% confidence level, an RMS error below 7.4 mm, and 5 mm resolution in a localization volume of $2 \times 2 \times 0.4\ \mathrm{m}^3$.**

***Index Terms*—Accurate localization, broadband transducers, Local Positioning Systems (LPSs), system evaluation, ubiquitous computing.**

I. Introduction

THE demand of new location-aware solutions for new necessities has triggered the research and development of new location platforms for accurate or physical localization (some interesting surveys can be found in [2] and [3]). The design of these platforms strongly depends on the application in mind, for example, to operate outdoor or indoors. The most prominent technology for outdoor environments is the NAVSTAR Global Positioning System (GPS), which is of limited use indoors [4]. Systems designed to operate indoors are usually referred to as Local Positioning Systems (LPSs) since they are designed for covering an enclosed area such as a building, a room, etc.

Recent research on positioning systems aims to improve the positioning accuracy. This can mainly be achieved by a precise estimation of the range between a beacon and a receiver; in particular, for GPS, by differential carrier-based ranging and trilateration techniques. The GPS technology is now able to obtain positioning errors as low as 20 mm with Real-Time Kinematics Differential GPS (DGPS-RTK) [5] in outdoor environments free of obstacles. LPSs based on Time of Flight (ToF) measurements such as Ultra-Wideband (UWB) achieve accuracies of tens of centimeters [6], [7]. LPSs based on Received Signal Strength Indicator (RSSI) such as several implementations using Wifi [8], RFID [9], or mobile networks have several meters of error. Artificial vision developments achieve accuracies of several centimeters [10]. Systems based on acoustic signals are able to attain accuracies of a few centimeters, with the most representatives being Active Bat [11], Cricket [12], SmartLocus [13], and Dolphin units [14].

Recently, in [1], a new advanced acoustic location system was presented by the authors of this paper. This LPS, which is called 3D-LOCUS, outperforms current acoustic LPSs by being able to precisely determine a mobile target position with subcentimeter accuracy. Additionally, 3D-LOCUS has the ability to compensate temperature gradients and airflows. Its accuracy is independent of the node's orientation, since transducers have a virtual point-like center of emission and reception. Its flexibility to work as a centralized, privacy-oriented, or bidirectional system, together with the parameterization of different access modes and signal designs, makes it easy to compare it to similar systems reported in the literature. The 3D-LOCUS distributed computing architecture is able to update the target position up to ten times per second in Code-Division Multiple-Access (CDMA) centralized mode.

In this paper, we present a complete evaluation of the performance of the 3D-LOCUS system. Section II presents a model for the 3D-LOCUS acoustic emission and reception process. Taking into account the expected ranging precision and its dependency with the properties of the signal, we design, according to this model, a good signal for emission and a proper sampling for reception. Section III evaluates the goodness of the 3D-LOCUS calibration method. It compares the estimated position of the transducers at every fixed node in several separate calibrations. Finally, in Section IV, the positioning performance obtained with this system is evaluated in terms of RMS errors and confidence levels while also taking into account several aspects, such as resolution and coverage, which

Manuscript received December 30, 2007; revised July 23, 2008. First published May 26, 2009; current version published July 17, 2009. The work of J. C. Prieto was supported by an I3P grant from the Consejo Superior de Investigaciones Científicas (CSIC). This work was supported by the Spanish Ministry of Science and Technology under PARMEI Project DIP2003-08715-C02-02. The Associate Editor coordinating the review process was Dr. Jesús Ureña.

J. C. Prieto, A. R. Jiménez, J. Guevara, F. Seco, and J. O. Roa are with the LOPSI Group, Instituto de Automática Industrial, Consejo Superior de Investigaciones Científicas (CSIC), 28500 Madrid, Spain (e-mail: cprieto@iai.csic.es).

J. L. Ealo is with the LOPSI Group, Instituto de Automática Industrial, CSIC, 28500 Madrid, Spain, and also with the School of Mechanical Engineering, Universidad del Valle, Cali 25360, Colombia.

F. Ramos was with the LOPSI Group, Instituto de Automática Industrial, CSIC, 28500 Madrid, Spain. He is now with NOVATRONIC, Quito, Ecuador.

Color versions of one or more of the figures in this paper are available online at http://ieeexplore.ieee.org.

Digital Object Identifier 10.1109/TIM.2009.2016378

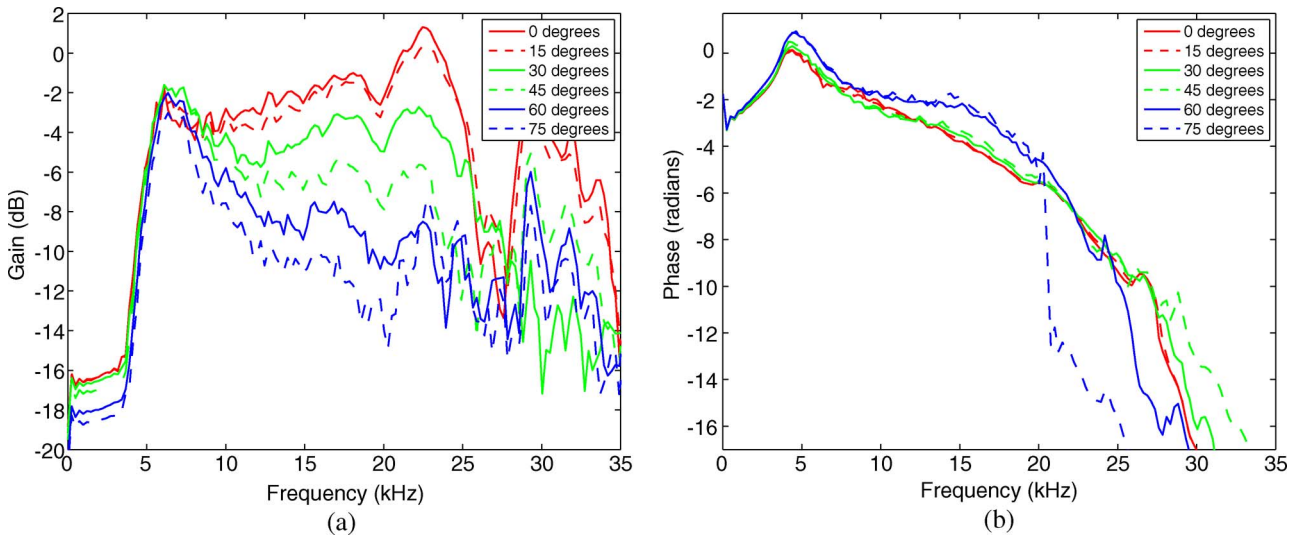

Fig. 1. Transfer functions that model the available bandwidth in the emission/reception process of the 3D-LOCUS system showing its dependence on the transducers' orientation. (a) Transfer function gain. (b) Transfer function phase.

are not usually evaluated in other LPS systems. A discussion and some conclusions are given in Section V.

II. Signal Parameter Selection

Sonic signals generated by 3D-LOCUS nodes are based on BPSK-modulated spreading Golay codes [15], specifically, preferred groups of unpaired codes [16]. These signals are correlated at the receiver for ToF estimation, which makes use of an efficient Golay correlator (EGC) [17]. The use of such signals improves the ranging accuracy and robustness against environmental noise and enables code-multiplexing schemes.

The use of full Golay pairs was not considered since it would make difficult the easy expansion of the system. In its current implementation, the system could receive and process full Golay signals since all the processing is implemented in software; but it only has enough hardware for emitting BPSK signals.

The main parameters selected for the emitted signal are the carrier frequency (f_c), the length of the sequence, and the number of carrier cycles per code chip. For reception, we need to select the sampling frequency (f_s). To obtain these parameters, we will consider a fixed signal-to-noise ratio and two models of the acoustic transmission channel.

An experimental identification of the transfer function of the ultrasonic channel was accomplished. This model includes, apart from the channel effect, the electronics and transducer influence on the signal. The transfer function was obtained by emitting a chirp signal from 0 Hz to 500 kHz, acquiring the received signal at a sampling rate of 1 MHz, and adjusting an IIR filter of order 10 by minimizing the output error, i.e., the difference between filter and system outputs. Fig. 1 shows the transfer function obtained at several orientations between emitter and receiver. Note that the usable bandwidth diminishes as obliqueness increases [Fig. 1(a)], but the effective bandwidth is about 20 kHz for most orientations considering a 6 dB band. The phase change [Fig. 1(b)] is quite smooth for the frequencies of interest (5–25 kHz) if the orientation between both transducers is equal or lower than 60°. At higher orientation angles, the phase response is worsened outside the 5–20 kHz window.

This transfer function was used for evaluating the influence of carrier, code, and sampling frequencies, as well as code length, on the precision of the measuring process. Fig. 2 shows the influence of the considered parameters on the variance of distance estimation. The study is performed by simulation using two transfer function models: 1) ideal (red circles), with infinite bandwidth, so that the received signal is the same as the emitted signal; and 2) the transfer function previously mentioned above (blue), identified for the 3D-LOCUS system, without rotation (asterisks), 30° rotation (squares), 45° rotation (diamonds), and 60° rotation (triangles). Signals are corrupted with additive white Gaussian noise to achieve an SNR of 12 dB.

This figure shows the main influence of the rotation angle on the range measurements: the increment of the variance. This influence also depends on the parameters of the signal, i.e., being more important for lower sampling frequencies, for instance.

Fig. 2(a) shows the influence of the modulating carrier frequency (f_c). The variance will decrease with higher frequencies in the ideal response, since the bandwidth of the resulting signal increases [18]. The filtered response will be more affected when the carrier approaches the band edges, since part of the signal will be filtered. The minimum of the variance depends on the model used. Since the higher frequencies are more affected by transducer rotation (as shown in Fig. 1), 15 kHz is chosen as a trade of frequency, which is valid for most orientations between transducers, for the modulating carrier.

Fig. 2(b) shows the influence of the number of carrier cycles used for modulating every code chip (carrier and code frequencies ratio). The number of cycles per chip defines the chip duration and, therefore, the signal bandwidth. We see that the ideal response is not affected when the signal bandwidth is increased (fewer cycles per chip). A good behavior for every

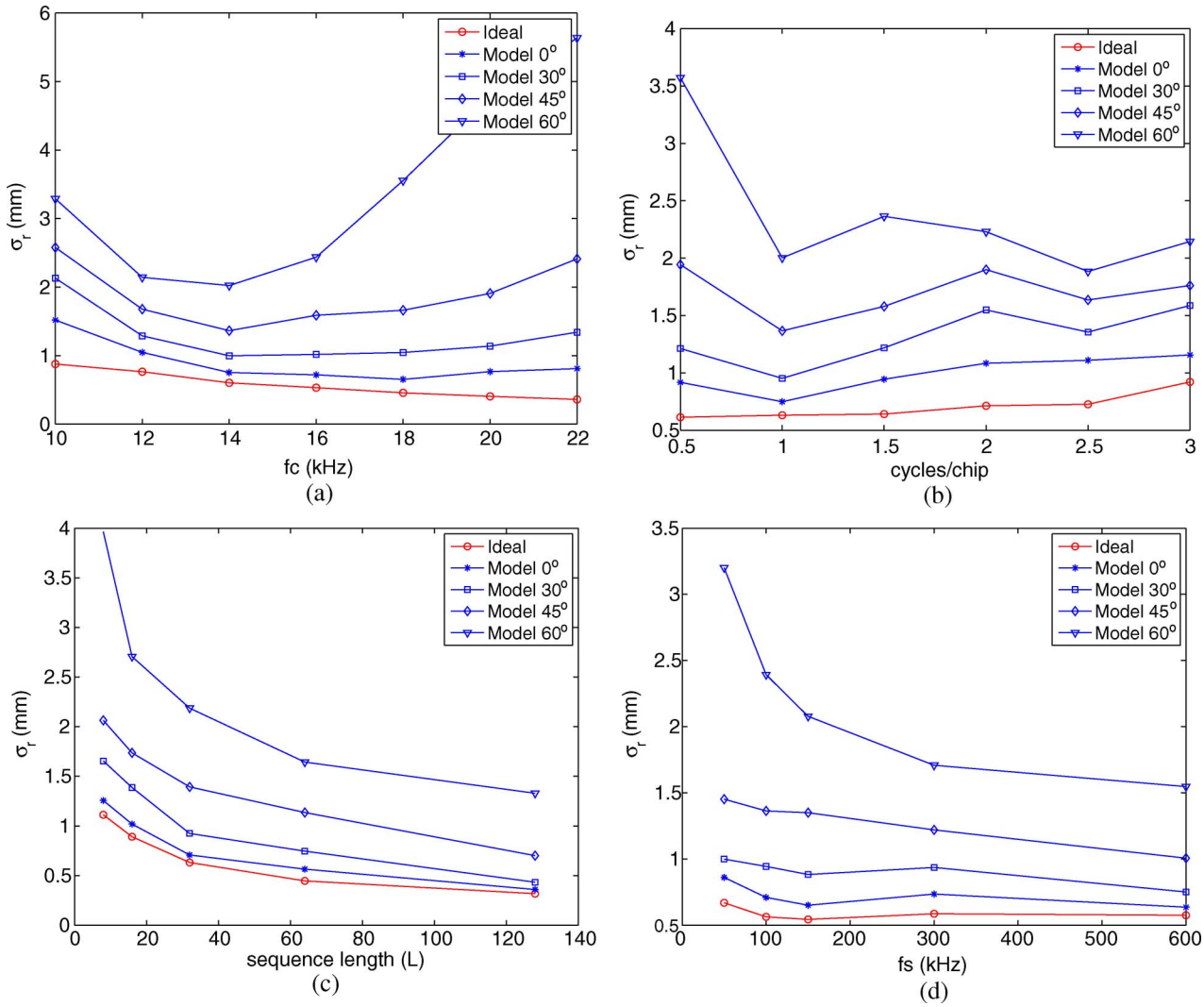

Fig. 2. Simulated ranging performance (standard deviation of range estimations) influenced by the selection of modulation, codification, and acquisition parameters. Default parameters: $f_c = 15$ kHz, $f_s = 150$ kHz, cycles/chip $= 1$, SNR $= 12$ dB, and L $= 32$ chips. (a) Carrier frequency. (b) Cycles per chip. (c) Sequence length. (d) Sampling frequency.

transducer's orientation is found using one or more cycles per chip. Therefore, to shorten the resulting signal as much as possible (for avoiding the effect of air turbulence), we use one cycle per chip.

When analyzing the ToF variance with respect to the length of the sequence, we find, as expected, that the longer is the sequence, the smaller is the variance [Fig. 2(c)]. However, taking into account possible turbulences, it is important to keep the duration of the signal short. The proper correlation of spread-spectrum-coded signals is very sensitive to turbulences in the air; fortunately, due to the dynamics of air, there is a time threshold for the duration of the signal (10 ms) that, if not surpassed, makes signal correlation quite robust against turbulences [19]. A good compromise between a short signal and a low variance is obtained using 32 chip long codes $(L = 32)$.

Finally, the variance will be lower with higher sampling frequencies (f_s) used in the receiver [Fig. 2(d)]; however, this implies more computation time. It can be noticed that, at frequencies below 100 kHz, the standard deviation of the ToF significantly grows for orientations higher than 60°. For guarantying good accuracy in most circumstances, 150 kHz is chosen as the sampling frequency. At this sampling rate, ten samples are used to digitize each carrier cycle.

Subsequent evaluation tests of 3D-LOCUS will use as the emitted signal a Golay code with 32 chips, which is modulated with 1 cycle per chip and a 15 kHz carrier. Acquisition will be performed at the receiver with a sampling frequency of 150 kHz. This signal design took into account the variable bandwidth, which depends on the transducer rotation, the expected influence of air turbulences, and the computational complexity of the receiver.

III. Node's Position Calibration Assessment

We deployed seven fixed wired nodes oriented downward in a robotic cell (2800 mm × 2800 mm × 2800 mm) (Fig. 3). One additional wired node was located inside the cell pointing upward. A Stäubli Unimation industrial robotic arm is used as reference for positioning a mobile wireless node fixed to its wrist as a tool, which is always oriented upward. These nodes are numbered from 1 to 9, where the number 3 is the mobile node, the number 6 is the fixed upward node, and the

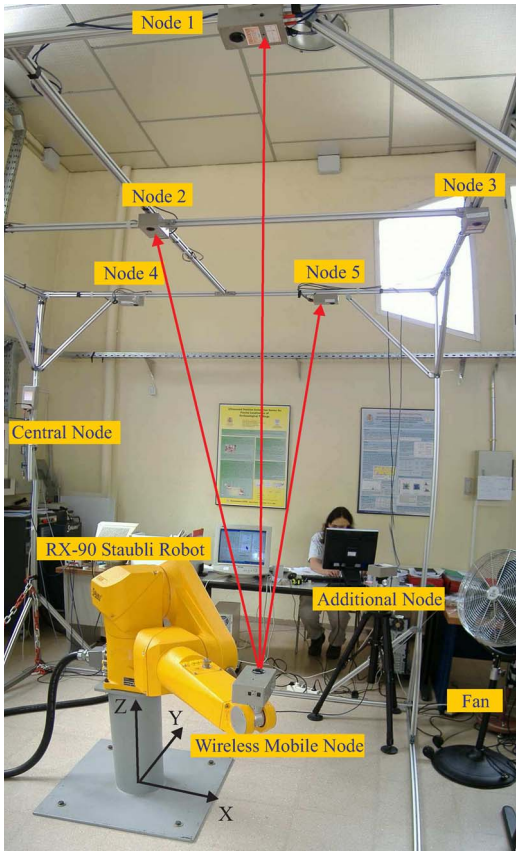

Fig. 3. Physical description of the actual implementation of the 3D-LOCUS system labeling its main components: fixed nodes in the structure, mobile node in the robot wrist, central node for measurement synchronization, and industrial fan for air perturbations.

rest correspond to the fixed downward nodes, which are also called beacons.

The calibration of the node's position was performed by positioning the wireless node in four points with the robot arm and measuring the ToFs to the emitter and the receiver of every node fixed to the cell structure. Three of these points were arranged to form an almost equilateral triangle, and the fourth is in its center at a different height. From these measurements, the sound velocity and the 3-D coordinates of every node's emitter and receiver were calculated, which was made considering the sound velocity as unknown in the trilateration equations [20], in the upward (1) and downward (2) propagation directions:

$$\widehat{V}_s ToF_{ij} = \sqrt{(\widehat{x}_{r_j} - x_{e_i})^2 + (\widehat{y}_{r_j} - y_{e_i})^2 + (\widehat{z}_{r_j} - z_{e_i})^2} \quad (1)$$

$$\widehat{V}_s ToF_{ji} = \sqrt{(\widehat{x}_{e_j} - x_{r_i})^2 + (\widehat{y}_{e_j} - y_{r_i})^2 + (\widehat{z}_{e_j} - z_{r_i})^2} \quad (2)$$

where

$\widehat{V}_s$	estimated sound velocity;
$ToF_{ij/ji}$	ToF measured from the mobile node at point i to the beacon j or in the other direction;
$(\widehat{x}_{e/r_j}, \widehat{y}_{e/r_j}, \widehat{z}_{e/r_j})$	estimated position or the transducers (e: emitter, r: receiver) of the fixed node j;
$(x_{e/r_i}, y_{e/r_i}, z_{e/r_i})$	known mobile transducers' (e: emitter, r: receiver) position at point i.

This algorithm minimizes the effect of environmental temperature drifts and gradients on positioning, since it determines an averaged value for the sound velocity without having to use a thermometer. If V_s is estimated with a temperature measurement, then it will depend on the spatial position where the temperature is measured, which could not fully correspond to the temperature of the path followed by the acoustic signal.

The consistency of calibration results was evaluated by repeating 11 independent node position calibrations. The variation of every $(\widehat{x}_{e/r_j}, \widehat{y}_{e/r_j}, \widehat{z}_{e/r_j})$ coordinate with respect to their mean is shown in Fig. 4 for emitters (first column) and receivers (second column). It can be noticed that the variability of the emitters is higher than that of the receivers. We believe that this effect is due to the higher omnidirectionality of the receivers that can capture some multipath produced in the robotic arm. The repetitiveness of the transducers' position is approximately bounded by ± 2 mm for emitters and ± 1 mm for receivers on every coordinate.

Since there is no real knowledge of the exact position of emitters and receivers, we considered an indirect procedure to estimate the calibration performance. The actual distance between both transducers' center on every node (64.11 mm) is used as an indication of calibration accuracy. Fig. 5(a) shows the distances obtained from the calibration data. The mean measured distance between both transducers, considering all the nodes, is about 64 mm, with variations of ± 4 mm. Fig. 5(b) shows the variability of the measured distance relative to the mean distance of every node, with variations of ± 2 mm. These results suggest that the calibration of the fixed node transducers' position is accurate at the millimeter level, and the system is ready for positioning evaluation.

IV. Positioning Evaluation

Most ultrasonic LPS evaluations only rely on the overall accuracy achieved by the system under some confidence level. In this section, a more detailed evaluation of the 3D-LOCUS positioning error will be presented, which takes into account the percentage of valid measurements, precision, trueness, RMS values, and overall error accuracy. Afterward, an analysis of the system resolution will be presented. Finally, an evaluation of the coverage of the system will be shown.

A. Positioning Error

For evaluating the error present in 3-D position estimation, three different configurations were considered.

1) Centralized: the nodes oriented upward act as emitters, and the nodes fixed downward act as receivers.
2) Privacy oriented: the nodes fixed to the cell structure act as emitters (i.e., sound waves propagate in the opposite direction than in the centralized mode).
3) Bidirectional: both ways sequentially.

In the last case, both emitter and receiver positions of the mobile node are determined. The average of both position estimations is considered as the resulting position of the node.

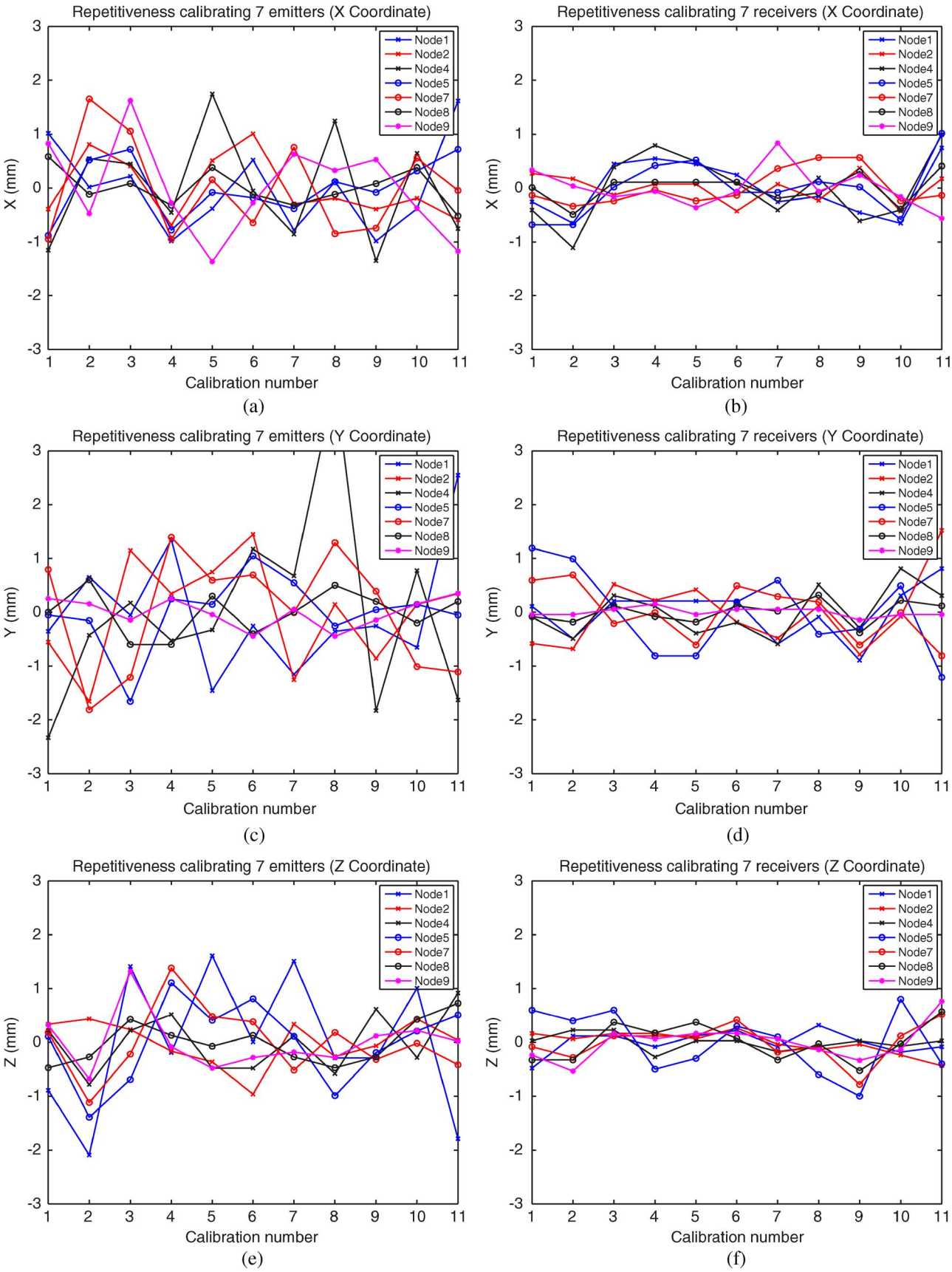

Fig. 4. Evaluation of the transducers' position consistency of the seven fixed nodes for 11 independent calibrations, showing the fluctuation of the position estimation of their emitters and receivers for every coordinate axes. (a) $\widehat{x}_{e_j}$ fluctuations. (b) $\widehat{x}_{r_j}$ fluctuations. (c) $\widehat{y}_{e_j}$ fluctuations. (d) $\widehat{y}_{r_j}$ fluctuations. (e) $\widehat{z}_{e_j}$ fluctuations. (f) $\widehat{z}_{r_j}$ fluctuations.

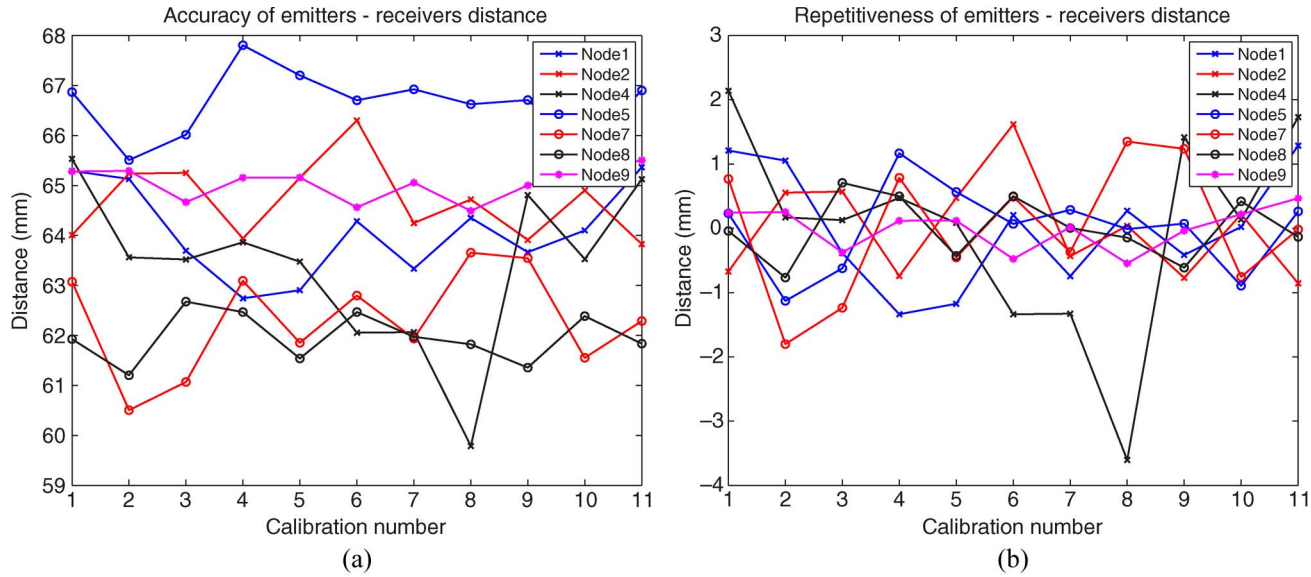

Fig. 5. Evaluation of the transducers' distance consistency of the seven fixed downward nodes for each of the 11 calibrations, showing the variation in distance obtained for separate nodes and its variation with different calibrations. (a) Distance between nodes' transducers. (b) Distance variation around their mean.

The following four test conditions were evaluated for every configuration:

1) time multiplexing (Time-Division Multiple Access, TDMA) (calm air);
2) code multiplexing (CDMA[1]) (calm air);
3) TDMA with airflows (fan stream at 2 m/s);
4) CDMA[1] with airflows (fan stream at 2 m/s).

The first condition is the most ideal case since neither wind disturbances nor signal interference is present. The CDMA mode presents signal degradation due to the interference among signals coming from different nodes. The potential deterioration of signal correlation that can be caused by air turbulence is minimized by the short signal length, as presented in Section II. However, airflows produce distance measurement degradation since the ToF varies when the propagation medium (air) moves (airflow).

CDMA measurements are degraded by two highly related factors: Multiple-Access Interference (MAI) and the near–far effect. The latter is due to power differences among the received signals from each emitting node. It was reduced enough to enable correct measurements, i.e., readjusting the emission power in every point in CDMA mode. The two upward nodes were tested by emitting the same power. The MAI errors are due to the cross-correlation properties of the codes (since they are not completely orthogonal) and worsened because of the near–far effect. In this paper, MAI was reduced by selecting a group of codes with good cross-correlation properties.

The update rate depends on the access mode (TDMA or CDMA) and the configuration. In TDMA mode, the signals are sequentially emitted from every node, requiring more time than in CDMA mode, where all the signals are simultaneously emitted. If 3D-LOCUS is configured to only transfer ToFs from the sensing nodes to the central node (fastest operation mode), then the update rate is 10 Hz in CDMA centralized mode (the higher) and 2 Hz in TDMA bidirectional mode (the lower). If the number of fixed nodes is duplicated, then the update rate would be 1 Hz in TDMA.

[1]Multiple-access configurations were tested with just four downward nodes.

TABLE I
TWENTY-TWO TEST POINTS CONSIDERED FOR SYSTEM EVALUATION

Position	x (mm)	y (mm)	z (mm)
1	-750	750	0
			200
			400
2	0	1060	0
			200
			400
3	750	750	0
			200
			400
4	1060	0	0
			200
			400
5	750	-750	0
			200
			400
6	0	-1060	0
			200
			400
7	-750	-750	0
			200
			400
8	0	0	550

For every configuration and test condition, 22 test positions were defined, and more than 100 measurements were made on each position. One position was in the center of the cell, and the remaining 21 were in seven different "xy" points around the robot at three different heights (differing by 200 mm). Table I defines the exact position of these 22 test points.

Position and sound velocity were estimated from (1) and (2) through a Levenberg–Marquardt algorithm, which minimizes the sum of the squared residuals, defined as the difference between both terms of the equations. A point located 1.5 m

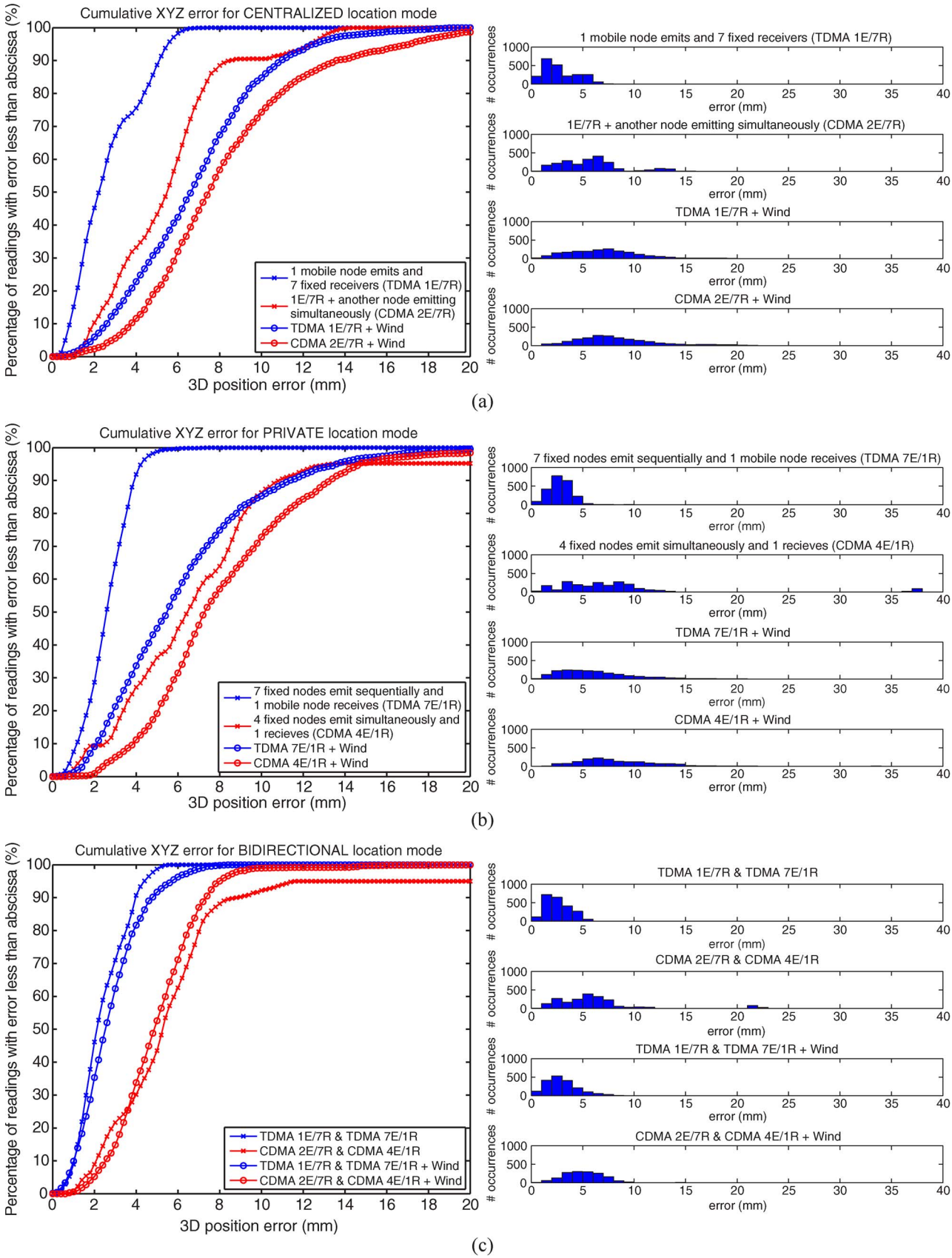

Fig. 6. Cumulative positioning error distributions and error histograms for the considered configurations under test conditions for the overall evaluation of system performance. (a) Centralized. (b) Privacy oriented. (c) Bidirectional.

TABLE II
VALID READINGS, 90% AND 95% CONFIDENCE LEVEL POSITIONING ERRORS, AND RMS ERRORS FOR THE CONSIDERED CONFIGURATIONS UNDER TEST CONDITIONS

Configuration		Valid Readings (%)	90% level error (mm)	95% level error (mm)	RMS (mm)
Centralized	TDMA	100	5.3	5.7	3.2
	CDMA	96.2	8.7	12.6	6.4
	TDMA W	90.4	11.1	12.7	7.7
	CDMA W	96.2	13.7	17.3	9.3
Private	TDMA	99.8	4.1	4.4	3
	CDMA	94.7	11.0	13.5	10.7
	TDMA W	89.5	11.6	13.8	7.4
	CDMA W	74.0	13.5	14.9	9.5
Bidirectional	TDMA	99.8	4.1	4.6	2.8
	CDMA	90.9	9.0	20.9	7.4
	TDMA W	84.4	5.0	5.9	3.3
	CDMA W	71.5	7.5	8.2	5.6

below the centroid of the beacons and a value for the velocity of sound of 340 m/s are used as the starting estimations of the algorithm. Estimations with residuals above 50 mm were considered as outliers and labeled as "non valid readings." These estimations are rejected by the system and not considered in the error distributions.

The obtained results are shown in Fig. 6 for every test condition, presenting the cumulative positioning error distributions and error histograms for the centralized [Fig. 6(a)], private [Fig. 6(b)], and bidirectional [Fig. 6(c)] configurations. These error distributions can be approximated by nonnormalized noncentral chi-square distributions with three degrees of freedom in every point. The numerical results extracted from these graphics are presented in Table II, which corresponds to the percentage of valid readings, absolute error achieved with 90% and 95% confidence levels, and RMS positioning errors.

The percentage of valid readings diminished as the disturbing conditions increase, i.e., changing from 100% to 71.5%. The privacy-oriented configurations returned less valid data than the centralized configurations. The bidirectional estimations are a combination of the previous positioning data; therefore, they will always return fewer valid measurements than either of the unidirectional configurations.

As expected, a poorer performance is found when the measurement disturbances increase (multiple access and wind). The system performance was less degraded by wind for CDMA modes of operation than those using TDMA (see the cumulative error distributions in Fig. 6). The presence of several outliers in private CDMA mode [visible in the error histograms of Fig. 6(b)] fails the general tendencies of absolute error and RMS in this mode and in bidirectional CDMA mode. The absolute error with 90% confidence level varies from 4.1 to 13.7 mm, and the RMS value varies from 2.8 to 10.7 mm.

The cumulative errors and the RMS values, under bidirectional configuration for windy conditions, were about half of the corresponding unidirectional modes. In a bidirectional configuration under every test condition, the 90% confidence level errors are under 10 mm, and the RMS values are below 8 mm.

For additional insight into the evaluation results, Table III shows the positioning errors along each individual coordinate axis. These results include the trueness measured as the mean of the error distribution and the covariance matrix. We have followed the recommendations of the standard ISO 5725 for the computation of trueness and variance (which corresponds to the precision value squared). The covariance values are almost always lower than the variance of the corresponding axes, which implies that the errors are partially coupled, as could be expected from a trilateration process under some geometries among nodes.

An evaluation of the system in outdoor environments was accomplished using TDMA operation modes. We checked the capability of 3D-LOCUS to compensate or diminish the wind-dispersive effect on position estimations with natural airflows, which is somehow different from the airflow produced with the industrial fan. This evaluation was made under natural wind streams with velocities of up to 3 m/s. The results obtained from these experiments showed a reduction in the final position dispersion in bidirectional mode of about 70%: from a standard deviation of 9.2 and 9.6 mm in centralized and private modes, respectively, to 3 mm in bidirectional mode. This reduction is more significant in the x and y coordinates (from 5.8 mm to 0.9 mm in the x coordinate, and similarly for the y coordinate) than in the z coordinate (from 5 to 2.7 mm). Therefore, we can say that the results are similar to those found indoor with a forced airflow, taking into account that this evaluation was made in a single point with unknown coordinates only evaluating the dispersion of the position estimation.

Along this analysis, the error evaluation area has been restricted to the space reachable by the robotic arm. The necessity for extending the evaluation area to wider spaces will require the definition of new methodologies for precisely locating the mobile test points, since they must be located with significantly better accuracy than that of our system (with an RMS error of 2.8 mm in the best case). A total station position measurement could be the substitution to the robot arm for extended areas. However, the real accuracy of a total station (between ± 1 and ± 3 mm) would not be as good as robot accuracy and could be closer to that observed in the system [21].

B. Resolution

System resolution is evaluated by generating a decreasing-side squared trajectory from 10 to 1 mm side length at 1 mm steps. This trajectory is performed by moving the mobile node with the robotic arm. The maximum resolution that the system would be able to offer will be the minimum discernible step in such a trajectory.

Fig. 7(a) shows the results obtained in TDMA mode without any perturbation, whereas Fig. 7(b) presents the results under wind perturbations. The trajectories estimated for the emitter (centralized mode), the receiver (private mode), and the bidirectional result, as well as the theoretical true trajectories, are presented in both figures.

TABLE III
COORDINATE AXES ERRORS: 90% AND 95% CONFIDENCE LEVEL ERRORS, TRUENESS, RMS ERRORS, AND COVARIANCES FOR THE CONSIDERED CONFIGURATIONS UNDER TEST CONDITIONS

Configuration		90% level error (mm)			95% level error (mm)			Trueness (mm)			RMS (mm)			Covariance (mm^2)					
		x	y	z	x	y	z	x	y	z	x	y	z	xx	yy	zz	xy	xz	yz
Centralized	TDMA	1.9	4.6	3.4	2.2	4.9	3.9	-0.5	-0.3	-0.3	1.2	2.2	2	1.1	4.9	3.9	-0.6	0.1	2
	CDMA	4.7	5.6	6.9	6.2	6.5	8.1	1	-0.9	-1.7	3.3	3.3	4.4	9.6	10.3	16.3	-1.4	0.3	-1.8
	TDMA W	6.7	8.4	6.4	8.4	9.8	7.8	-0.5	-3.3	-1.7	4.1	5.2	3.9	16.8	16.1	12.3	-0.4	-1.8	4.3
	CDMA W	10.4	9.3	6.8	12.8	11.4	7.7	-0.9	-3.8	-1.4	6.3	5.6	3.9	38.9	17.2	13.6	-6.4	-5.1	4.1
Private	TDMA	2.4	3	3	2.8	3.5	3.6	-0.8	-0.1	-0.2	1.5	1.8	1.9	1.5	3.1	3.6	-0.5	0.1	-0.4
	CDMA	7.4	7.5	6.1	11.1	8.9	9.2	2.3	-2.1	-0.3	8.5	4.6	4.5	67.3	17.1	20	-2.7	21.2	-3
	TDMA W	6.3	7.8	6.4	7.9	10.5	8	-0.7	2.5	1.4	4	4.8	3.9	15.9	16.4	13.5	-0.5	-1.1	0.8
	CDMA W	10	9.1	7	12.8	10.3	8.2	1.6	1.8	1.8	6.1	5.8	4.5	35.2	29.9	16.9	-7.1	4.5	0.6
Bidirectional	TDMA	1.9	3.9	2.7	2.2	4.1	3.1	-0.7	-0.2	-0.3	1.2	1.9	1.7	0.9	3.5	2.8	-0.5	0.2	0.7
	CDMA	6	5	4.9	20.3	6.6	5.5	1.7	-1.5	-0.8	5.5	3.4	3.5	27.6	9.4	11.8	-2.9	4.7	-5.4
	TDMA W	2.6	3.3	3.5	3.3	4.4	4.1	-0.4	-0.5	-0.1	1.6	1.9	2.2	2.3	3.5	4.6	-0.3	0	0.1
	CDMA W	5.1	5	5.3	6	5.9	5.8	0.4	-0.8	0.1	3.2	3.1	3.3	10.2	9	10.9	-2.6	2.1	-1.6

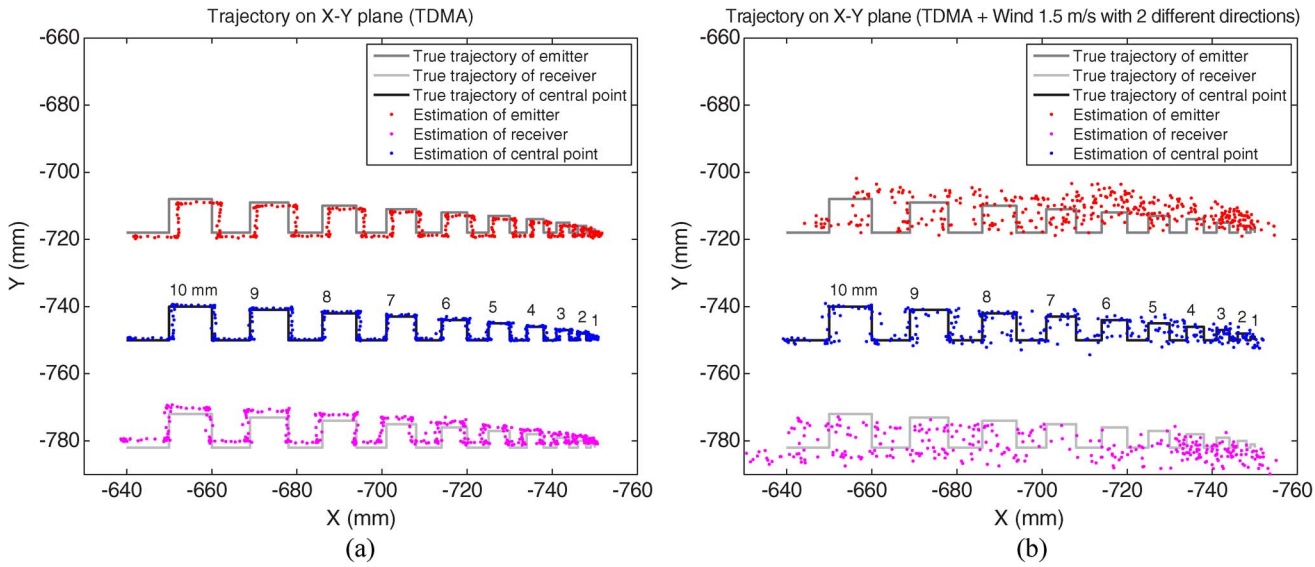

Fig. 7. Stair-stepped squared trajectory described by the mobile node in TDMA mode for resolution evaluation (minimum discernible step). Trajectories followed by emitter, receiver, and central point correspond to centralized (red), privacy oriented (pink), and bidirectional (blue) configurations, respectively. (a) Without wind. (b) Under wind disturbances.

The results shown in Fig. 7(a) indicate that, without any perturbation, it is possible to distinguish 2 mm steps on every trajectory. Under airflow conditions, the attained resolution is about 10 mm for private and centralized mode and about 5 mm in bidirectional mode. Therefore, the bidirectional operation mode in 3D-LOCUS is good not only for achieving subcentimeter positioning error but also for obtaining a good resolution.

The system resolution was also evaluated for CDMA operation, finding that the 3D-LOCUS system was not able to follow the trajectory in this mode due to many nonvalid estimations. This is because of the fact that neither a MAI cancellation scheme nor an automatic adaptation of the emission power has been implemented up to now in the 3D-LOCUS system.

C. Coverage

The capacity of the system to make measurements outside the robotic cell was evaluated by manually moving the mobile node following a zig-zag trajectory. This system is able to localize far from the cell due to the omnidirectional characteristics of their transducers [1]. This evaluation was performed in just one quadrant, considering that the obtained results can be extrapolated to the remaining three.

Fig. 8 shows the result obtained. It can be appreciated an approximately circular coverage area of 4 m radius (circular dotted line). The system accuracy is lower in this area due to the poorer geometry (high Geometric Dilution of Precision (GDOP) [22]), the higher dispersion in ToF measurements due

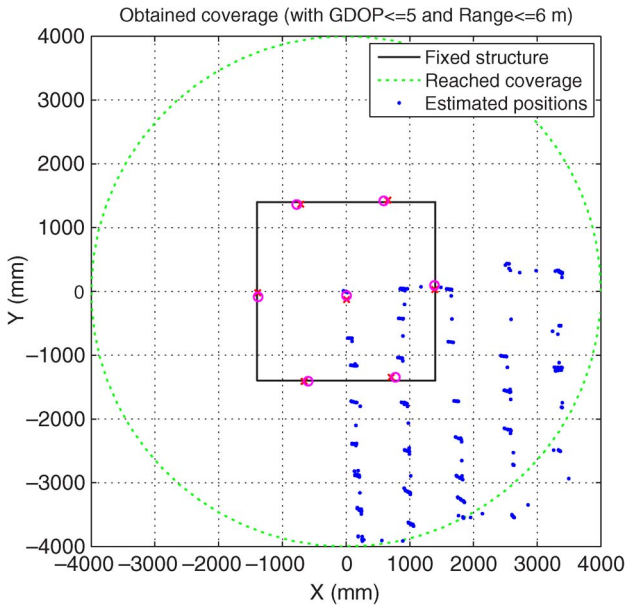

Fig. 8. Coverage obtained when manually moving the mobile node outside the robotic cell. The seven fixed downward nodes are represented by a red circle and a cross (emitter and receiver of each node, respectively).

to an increase of the orientation between transducers, and the longer propagation times.

This result does not imply that the best configuration for covering this area is the one presented, it just offers an evaluation of the capability of the nodes for covering areas not enclosed by them, and this feature is enabled by the good directionality pattern of the selected transducers and the rotational invariance of the range measurements [1]. The practical consequence is that the node density necessary for obtaining complete coverage in a final deployment can be very low. The evaluation of the maximum area that could be covered separating these seven nodes has to be studied.

V. Conclusion

The evaluation of the 3D-LOCUS acoustic LPS has been presented. The main parameters involved on signal emission and reception were selected for accurate ranging, taking into account the bandwidth and directionality of the transducers. The calibration process for fixed nodes' position determination was evaluated, finding it repetitive and accurate. The 3D-LOCUS positioning performance was evaluated by considering several important aspects that are not usually reported with enough detail in other LPS evaluations. Apart from the absolute error and the valid reading evaluation, a measure of trueness, precision, RMS error, resolution, and maximum attainable coverage was offered.

The 3D-LOCUS system, in bidirectional mode, has subcentimeter accuracy (RMS errors below 8 mm), is able to reach 5 mm resolution, and possesses a wide coverage. These results are also valid even under moderate airflows. Therefore, the implemented system outperforms (in terms of accuracy, resolution and coverage) those LPSs found on the bibliography. 3D-LOCUS could be considered as the first subcentimeter-accuracy acoustic LPS usable in both indoor and outdoor environments, and it is a flexible platform to test future research on precise positioning.

Acknowledgment

The authors would like to thank the suggestions of the anonymous reviewers.

References

[1] J. C. Prieto, A. R. Jiménez, J. I. Guevara, J. L. Ealo, F. A. Seco, J. O. Roa, and F. X. Ramos, "Subcentimeter-accuracy localization through broadband acoustic transducers," in *Proc. IEEE Int. Symp. Intell. Signal Process.*, Alcalá de Henares, Spain, Oct. 3–5, 2007, pp. 929–934.

[2] J. Hightower and G. Borriello, "Location systems for ubiquitous computing," *Computer*, vol. 34, no. 8, pp. 57–66, Aug. 2001.

[3] A. R. Jiménez, F. Seco, R. Ceres, and L. Calderón, *Absolute Localization Using Active Beacons: A Survey and IAI-CSIC Contributions*, 2004. [Online]. Available: http://www.iai.csic.es/lopsi/static/phdteaching.htm

[4] P. Mattos, "Acquiring sensitivity to bring new signals indoors," *GPS World*, vol. 15, no. 5, pp. 28–33, May 2004.

[5] H. Baertlein, B. Carlson, R. Eckels, S. Lyle, and S. Wilson, "A high-performance, high-accuracy RTK GPS machine guidance system," *GPS Solut.*, vol. 3, no. 3, pp. 4–11, Jan. 2000.

[6] R. J. Fontana, "Recent applications of ultra wide band radar and communications systems," Multispectral Solutions, Germantown, MD, 2000, Tech. Rep.

[7] C. Falsi, D. Dardari, L. Mucchi, and M. Z. Win, "Time of arrival estimation for UWB localizers in realistic environments," *EURASIP J. Appl. Signal Process.*, vol. 2006, no. 1, p. 152, Jan. 2006.

[8] P. Bahl and V. N. Padmanabhan, "Radar: An in-building user location and tracking system," in *Proc. IEEE INFOCOM*, 2000, vol. 2, pp. 775–784. Tel Aviv, Israel.

[9] L. M. Ni, Y. Liu, Y. C. Lau, and A. P. Patil, "Landmarc: Indoor location sensing using active RFID," *Wirel. Netw.—Special Issue Pervasive Comput. Commun.*, vol. 10, no. 6, pp. 701–710, Nov. 2004.

[10] J. Krumm, S. Harris, B. Meyers, B. Brumitt, M. Hale, and S. Shafer, "Multi-camera multiperson tracking for easyliving," in *Proc. 3rd IEEE Int. Workshop VS*, 2000, pp. 3–10.

[11] A. Harter, A. Hopper, P. Steggles, A. Ward, and P. Webster, "The anatomy of a context-aware application," in *Proc. 5th Annu. ACM/IEEE Int. Conf. Mobicom*, 1999, pp. 1–59.

[12] H. Balakrishnan and N. Priyantha, "The Cricket indoor location system: Experience and status," in *Proc. WorkShop Location-Aware Comput. Ubicomp*, 2003, vol. 1, pp. 7–9.

[13] C. Brignone, T. Connors, G. Lyon, and S. Pradhan, "SmartLOCUS: An autonomous, self-assembling sensor network for indoor asset and systems management," Mobile Media Syst. Lab., HP Laboratories, Palo Alto, CA, Tech. Rep. 41, 2003.

[14] M. Hazas and A. Hopper, "Broadband ultrasonic location systems for improved indoor positioning," *IEEE Trans. Mobile Comput.*, vol. 5, no. 5, pp. 536–547, May 2006.

[15] M. J. E. Golay, "Complementary series," *IRE Trans. Inf. Theory*, vol. IT-7, no. 2, pp. 82–87, Apr. 1961.

[16] C. De Marziani, J. Ureña, M. Mazo, Á. Hernández, and J. M. Villadangos, "Algoritmo de posicionamiento en sistemas de localización de redes de sensores acústicos inteligentes," in *Proc. Int. Conf. TELEC*, Santiago de Cuba, Cuba, Jul. 14–16, 2004.

[17] B. M. Popovic, "Efficient Golay correlator," *Electron. Lett.*, vol. 35, no. 17, pp. 1427–1428, Aug. 1999.

[18] E. Weinstein and A. J. Weiss, "Fundamental limitations in passive time-delay estimation—Part II: Wide-band systems," *IEEE Trans. Acoust., Speech, Signal Process.*, vol. ASSP-32, no. 5, pp. 1064–1078, Oct. 1984.

[19] F. J. Alvarez, J. Ureña, M. Mazo, A. Hernández, J. J. García, and C. Marziani, "High reliability outdoor sonar prototype based on efficient signal coding," *IEEE Trans. Ultrason., Ferroelectr., Freq. Control*, vol. 53, no. 10, pp. 1862–1872, Oct. 2006.

[20] F. Morgado, A. R. Jiménez, and F. Seco, "Ultrasound-based 3d-coordinate measuring system for localization of findings in paleo-archaeological excavations," in *Proc. WAC/ISIAC*, Seville, Spain, Jun. 28–Jul. 1, 2004, vol. 16, pp. 216–222.

[21] Trimble, *Trimble 3600 Total Station*, 2007. [Online]. Available: http://trl.trimble.com//docushare/dsweb//Get/Document-10325/12414C_3600wTCU_DS_0507_lr.pdf

[22] R. Yarlagadda, I. Ali, N. Al-Dhahir, and J. Hershey, "GPS GDOP metric," *Proc. Inst. Elect. Eng.—Radar Sonar Navig.*, vol. 147, no. 5, pp. 259–264, Oct. 2000.

José Carlos Prieto was born in León, Spain, in 1978. He received the Technical degree in industrial electronics and the B.S. degree in electronics engineering from the Universidad de Extremadura, Badajoz, Spain, in 1999 and 2003, respectively, and the Master's degree in robotics from the Universidad Politécnica de Madrid, Madrid, Spain, in 2007. He is currently working toward the Doctoral degree in robotics with the Universidad de Alcalá, Madrid.

Since 2004, he has been a Researcher with the Instituto de Automática Industrial, Consejo Superior de Investigaciones Científicas (CSIC), Madrid. His research interests are focused in localization systems, mainly those based in ultrasonic signals, with special emphasis in signal design and processing, positioning algorithms, robustness, standardization, optimal configurations, calibration methods, and development of new transducers.

Antonio Ramón Jiménez received the degree in physics and computer science and the Ph.D. degree in physics from the Universidad Complutense de Madrid, Madrid, Spain, in 1991 and 1998, respectively.

From 1991 to 1993, he worked in industrial laser applications with the Technological Center of Madrid (CETEMA), Madrid. Since 1994, he has been a Researcher with the Instituto de Automática Industrial, Consejo Superior de Investigaciones Científicas (CSIC), Madrid. His current research interests include sensor systems (ultrasound and RFID) and algorithmic solutions for localization and tracking of persons or objects in sectors such as robotics, vehicle navigation, and ambient assistive living.

Jorge Guevara was born in Lima, Peru, in 1978. He received the B.S. degree in electronics engineering from the Universidad Católica Nuestra Señora de la Asunción, Asunción, Paraguay, in 2004. He is currently working toward the Ph.D. degree in electric engineering with the Instituto de Automática Industrial, Consejo Superior de Investigaciones Científicas (CSIC), Madrid, Spain.

His research interests are in the area of localization systems, in particular, automatic calibration methods for ultrasonic positioning systems.

Joao L. Ealo was born in Cartagena de Indias, Colombia, in 1976. He received the B.Sc. degree in mechanical engineering from the University of Ibagué, Ibagué, Colombia, in 1998 and the M.Sc. degree in industrial control systems from the University of Valladolid, Valladolid, Spain, in 2000. He is currently working toward the Doctorate degree in mechanical engineering with the Polytechnic University of Madrid, Madrid, Spain, supported by the Instituto de Automática Industrial, Consejo Superior de Investigaciones Científicas (CSIC), Madrid, and the University of Valle, Cali, Colombia.

He has been a tenured Lecturer in mechanical design with the School of Mechanical Engineering, University of Valle, since 2002. His current research interests are focused on the modeling and design of ultrasonic transducers for air-coupled applications, particularly in the fields of nondestructive testing, acoustic imaging, and local positioning systems.

Fernando Seco was born in Madrid, Spain, in 1972. He received the degree in physics from the Universidad Complutense of Madrid, Madrid, in 1996 and the Ph.D. degree in physics from the Universidad Nacional de Educación a Distancia (UNED), Madrid, in 2002. His dissertation dealt with the generation of ultrasonic waves applied to a magnetostrictive linear position sensor.

Since 1997, he has been with the Instituto de Automática Industrial, Consejo Superior de Investigaciones Científicas (CSIC), Madrid, where he holds a research position. His main research interest lies in the design and development of local positioning systems (LPS), particularly those based on ultrasound and RFID, and specifically on the topics of signal processing of ultrasonic signals, multilateration algorithms, and Bayesian localization methods.

Javier O. Roa was born in Colombia, in 1975. He received the Technical Electronic Engineer degree from the Unidades Tecnológicas de Santander, Bucaramanga, Colombia, in 1996 and the degree in electronic engineering from the Universidad del Valle, Cali, Colombia, in 2003. He is currently working toward the Ph.D. degree in electronics with the Universidad de Alcalá, Madrid, Spain.

Since 2004, he has been a Researcher with the Instituto de Automática Industrial, Consejo Superior de Investigaciones Científicas (CSIC), Madrid. His current research interests are in the field of optimization methods using metaheuristic techniques and concepts of artificial intelligence, such as evolutionary algorithms, fuzzy logic, and artificial neural networks.

Francisco Ramos was born in Ecuador, in 1979. He received the degree in electronic engineering from Escuela Politécnica Nacional de Ecuador, Quito, Ecuador in 2003 and the Master's degree in robotics from the Universidad Politécnica de Madrid, Madrid, Spain, in 2006.

From 2005 to 2006, he was with the Instituto de Automática Industrial, Consejo Superior de Investigaciones Científicas (CSIC), Madrid. He currently runs a company that works on electrical and electronic engineering projects in Ecuador.